BBA - General Subjects 1864 (2020) 129683

Contents lists available at ScienceDirect

BBA - General Subjects

journal homepage: www.elsevier.com/locate/bbagen

Potential antitumor activity of digitoxin and user-designed analog administered to human lung cancer cells

Reem Eldawud[a,1], Alixandra Wagner[a,1], Chenbo Dong[a], Neha Gupta[a], Yon Rojanasakul[b], George O'Doherty[c], Todd A. Stueckle[d,*], Cerasela Zoica Dinu[a,**]

[a] Department of Chemical and Biomedical Engineering, West Virginia University, Morgantown, WV 26506, USA
[b] Department of Basic Pharmaceutical Sciences, West Virginia University, Morgantown, WV 26506, USA
[c] Department of Chemistry and Chemical Biology, Northeastern University, Boston, MA 02115, USA
[d] Health Effects Laboratory Division, National Institute for Occupational Safety and Health, Morgantown, WV 26505, USA

ARTICLE INFO

Keywords:
Cardiac glycosides
Digitoxin
Synthetic analog
Lung cancer
Chemotherapy
Anti-tumor activity
Therapeutic alternatives

ABSTRACT

Background: Cardiac glycosides (CGs), such as digitoxin, are traditionally used for treatment of congestive heart failure; recently they also gained attention for their anticancer properties. Previous studies showed that digitoxin and a synthetic L-sugar monosaccharide analog treatment decreases cancer cell proliferation, increases apoptosis, and pro-adhesion abilities; however, no reports are available on their potential to alter lung cancer cell cytoskeleton structure and reduce migratory ability. Herein, we investigated the anticancer effects of digitoxin and its analog, digitoxigenin-α-L-rhamnoside (D6MA), to establish whether cytoskeleton reorganization and reduced motility are drug-induced cellular outcomes.

Methods: We treated non-small cell lung carcinoma cells (NSCLCs) with sub-therapeutic, therapeutic, and toxic concentrations of digitoxin and D6MA respectively, followed by both single point and real-time assays to evaluate changes in cellular gene and protein expression, adhesion, elasticity, and migration.

Results: Digitoxin and D6MA induced a decrease in matrix metalloproteinases expression via altered focal adhesion signaling and a suppression of the phosphoinositide 3-kinases / protein kinase B pathway which lead to enhanced adhesion, altered elasticity, and reduced motility of NSCLCs. Global gene expression analysis identified dose-dependent changes to nuclear factor kappa-light-chain-enhancer, epithelial tumor, and microtubule dynamics signaling.

Conclusions: Our study demonstrates that digitoxin and D6MA can target antitumor signaling pathways to alter NSCLC cytoskeleton and migratory ability to thus potentially reduce their tumorigenicity.

Significance: Discovering signaling pathways that control cancer's cell phenotype and how such pathways are affected by CG treatment will potentially allow for active usage of synthetic CG analogs as therapeutic agents in advanced lung conditions.

1. Introduction

Cardiac glycosides (CGs) are commonly used for the treatment of congestive heart failure and arterial fibrillation [1,2]. Previous research has shown that CGs block Na + /K + -ATPase pump activity [3] causing an increase in intracellular calcium thus allowing for more efficient contractions to occur [4]. Complementary research has also showed that CGs and user-synthesized analogs possess anticancer activities, with studies demonstrating their selectivity toward different cancer cells, from breast to lung cancer cell lines [2,5,6,7,8]. Within this context, we have previously compared digitoxin, a naturally occurring CG with a prolonged half-life in human serum [7] and an L-sugar monosaccharide analog of digitoxin, digitoxigenin-α-L-rhamnoside (D6MA, see Appendix A) [7,9] and identified that D6MA displayed a 5-

Abbreviations: AFM, atomic force microscopy; BCA, bicinchoninic acid assay; CG, cardiac glycoside; D6MA, digitoxigenin α-L-rhamnose monosaccharide; DTX, digitoxin; DEG, differentially expressed gene; E, Young's modulus; ECIS, electric cell impedance sensing; MFI, mean fluorescent intensity

* Correspondence to: T.A. Stueckle, Health Effects Laboratory Division, National Institute for Occupational Safety and Health, 1095 Willowdale Road, Morgantown, WV 26505, USA.

** Correspondence to: C.Z. Dinu, Department of Chemical and Biomedical Engineering, West Virginia University, Benjamin M. Statler College of Engineering and Mineral Resources, PO Box 6102, Morgantown, WV 26506, USA.

[1] Authors have contributed equally to this work.

https://doi.org/10.1016/j.bbagen.2020.129683
Received 24 March 2020; Received in revised form 19 June 2020; Accepted 9 July 2020
Available online 15 July 2020
0304-4165/ Published by Elsevier B.V.

fold increase in potency relative to its digitoxin counterpart [6], with such anticancer activity occurring in the nanomolar range thus helping to alleviate concerns over potential cardiotoxicity at administration [7,10]. Our analyses were performed in non-small cell lung carcinoma cells (NSCLC) lines due to their known resistance against drug therapies, high associated death rates relative to other cancers [6,7,10], and an increased sensitivity to digitoxin and its analogs toward such cells when compared to other studied cell lines [7,11].

In investigating the anticancer mechanisms associated with digitoxin and its analogs, we and others have attributed the drugs' effects to the ability of such compounds to activate downstream signaling pathways that regulate cellular proliferation [6,7,12], as well as the increase in anoikis via Mcl-1 degradation (an anti-apoptotic protein) associated with the GSK-3β-mediated signaling and deregulation of the mitochondria apoptotic pathway [10]. Published reports showed that NSCLCs treated with digitoxin and its analogs displayed G1/S or G2 arrests [6], inhibition of genes associated with cell proliferation (i.e., p53, cdc2, cyclin B1, survivin, and Chk1/2) [6], and pro-adhesion effects through enhanced CDK4/ZONAB/ZO-1 signaling [13], sensitization to tumor necrosis factor (TNF)-related apoptosis-inducing ligand (Apo2L/TRAIL) [2], as well as induced cellular apoptosis [9]. However, while such studies hint at the narrow therapeutic window of CGs or synthetic analogs, they do not provide indication on the ability of such compounds to alter cancer cell dynamics and induce their apoptosis.

We hypothesize that cellular transformation and anticancer mechanisms occur following digitoxin and D6MA exposure in human NSCLCs through re-organization of the cancer cell cytoskeleton and reduction in its migration capabilities. Such induced effects are envisioned to lead to re-establishment of cell-cell and cell-substrate connections to account for a transition of the cancerous cell to a more epithelial-like profile. To demonstrate our hypotheses we used NCI-H460 cells as NSCLC models because of their known increased resistance to chemotherapy [14]. The selected models were treated with sub-therapeutic, therapeutic, and toxic concentrations of digitoxin with equipotent doses of D6MA for anti-lung cancer therapy. The selectivity of digitoxin and D6MA toward NCI-H460 cells over non-malignant human bronchial epithelial cells (BEAS-2B) was verified using both single point and real-time assay via electric cell-substrate impedance sensing (ECIS). The anticancer mechanisms of both digitoxin and D6MA were evaluated via established *in vitro* cellular-based assays and quantitative analysis of the changes in gene and protein expression, with the hypothesis verified for an exposure to sub-therapeutic concentrations of both drugs. We envision that discovering the signaling pathways that control the phenotype of cancerous cells and how such pathways are affected by exposure to CGs or synthetic analogs will allow for active usage of these compounds as therapeutic agents in advanced lung conditions.

2. Methods

2.1. Synthesis of D6MA

D6MA, α-L-rhamnose monosaccharide was synthesized from digitoxin (Sigma) according to previously described methods [5,6,7,10,15–17]. Briefly, the trisaccharide moiety in digitoxin was cleaved by acid hydrolysis reaction to generate free aglycone moiety, i.e., digitoxigenin. Subsequently, the monosaccharide group was synthesized by a palladium-glycosylation (between digitoxigenin and a α-L-BocO-pyranone 1 to 2), [18] Luche reduction ($NaBH_4/CeCl_3$, 2 to 3) and Upjohn dihydroxylation (OsO_4/NMO, 3 to D6MA) to generate digitoxin-α-L-rhamnoside (D6MA; Supporting Information Scheme 2). Yields along the four-step process ranged between 70 and 90%, with good overall yield of 58% [19,20]. Details on D6MA synthesis can be found in Supporting Information.

2.2. Cell culture and treatment

Human non-small cancer lung cells (NCI-H460) and non-tumorigenic human lung epithelial cells (BEAS-2B) were purchased from American Type Culture Collection (ATCC). NCI-H460 cells were cultured in Roswell Park Memorial Institute (RPMI; Gibco) 1640 medium supplemented with 10% fetal bovine serum (FBS, Life Technologies), 2 mM L-glutamine and 100-units/mL penicillin/streptomycin (Sigma). BEAS-2B cells were cultured in Dulbecco's Modified Eagle Medium (DMEM; Sigma) supplemented with 5% FBS, 2 mM L-glutamine and 100-units/mL penicillin/streptomycin. Cells were passaged regularly using 0.25% (*w/v*) trypsin with 1.5 mM ethylenediaminetetraacetic acid (EDTA; Molecular Probes) and maintained in a humidified atmosphere at 37 °C and 5% CO_2. Stock concentrations of digitoxin and D6MA were prepared in sterile dimethyl sulfoxide (DMSO, Fisher) and diluted 1000x to obtain the exposure concentrations used in the experiments [6]. Digitoxin and D6MA exposures were performed in a medium containing 1% FBS, 2 mM L-glutamine, and 100 units/mL penicillin/streptomycin. The reduced concentration of FBS was adopted to circumvent existing concerns regarding potential digitoxin or D6MA interactions with serum proteins normally present in the media [21].

2.3. Electric cell impedance sensing (ECIS)

Real-time analysis of the cellular behavior was performed using an electric cell impedance sensing system (ECIS 96 W, Applied Biophysics). In each experiment, a 96W10idf ECIS array (Applied Biophysics) containing 96 wells each with 10 gold electrodes was used to provide concomitant measurements of 2000–4000 cells per well and at multiple frequencies. Prior to any experiment, the ECIS gold electrodes were stabilized for 3 h in 200 μL RPMI or DMEM media to create a reference line associated with free electrodes; subsequently, NCI-H460 or BEAS-2B cells were seeded at a density of 2×10^5 cell/mL in a volume of 200 μL/well. Cells were allowed to settle and grow over such media stabilized gold electrodes and form a confluent monolayer for 24 h. Subsequently, the cells were treated with 0, 10, 25, 50 and 100 nM digitoxin or 0, 1, 5, 10 and 25 nM D6MA and their cellular behavior post-exposure was monitored in real-time for an additional 48 h. DMSO-only (< 0.1% *v*/v) treated cells served as negative controls. Different dose ranges were chosen based on our previous work showing an about 5-fold difference in potency on NCI-H460 toxicity between the two compounds. The resistance of the cells on the electrodes (i.e., herein considering cells as insulators) along with the alpha parameter which details the current through the ventral surfaces of the cells and electrodes [22] were recorded every 12 min. Experiments were repeated 4 times with 2 replicates each, for a total of 8 replicates.

2.4. Cell size analysis

NCI-H460 cells were seeded overnight in 12-well plates (Fisher) at a density of 2×10^5 cell/well and treated with digitoxin (10, 25 and 50 nM) or D6MA (1, 5 and 10 nM) after they were allowed to form a confluent monolayer for 24 h. The cells were subsequently collected, washed with Phosphate Buffered Saline (PBS, Fisher) and analyzed for mean fluorescent intensity (MFI) using a BD LSR Fortessa Flow cell analyzer (BD Biosciences). A calibration curve was formed using beads with average diameters of 10.5, 14.7, 24.9 and 50 μm (Molecular Probes). For each sample, at least 20,000 events were collected using BD FACS Diva software (Verity Software House) and analyzed using FlowJo software V10.0.7 (Tree Star Inc.). Experiments were repeated 3 times, each with 3 replicates for a total of 9 replicates.

2.5. Biomechanical analysis

NCI-H460 cells were seeded overnight in 50 mm × 9 mm parallel culture Petri dishes (BD Biosciences) at a density of 1×10^6 cells/dish

and allowed to form a confluent monolayer. Subsequently, the cells were treated with digitoxin (10, 25, and 50 nM) or D6MA (1, 5 and 10 nM) for 24 h. A MFP-3D-BIO atomic force microscope (AFM; Asylum Research, TE2000-U) was used to evaluate biomechanical properties of the control (untreated) and treated cells. The location of the AFM cantilever was confirmed using a 10x objective.

Cellular elasticity was evaluated using Sneddon's modification of the Hertz model developed for a four-sided pyramid [23–25]. Force–displacement curves obtained during elastic mapping were converted into force-indentation curves [26] based on the assumption that the indented sample is extremely thick when compared to the indentation depth [27]. The cells elasticity (Young's modulus, E) was corrected with the indentation of the tip, δ through the following equation:

$$E = \frac{\pi}{2}\frac{1-\nu^2}{\tan\alpha}\frac{F}{\delta^2}$$

where the Poisson's ratio v for the cell was considered to be 0.5 [25] and $\alpha = 36^{\circ}$ was the open angle of the tip. The cantilever loading force F was obtained from simultaneously recording deflection of the cantilever and multiplying that by the cantilever spring constant (k = 0.09 N/m). Experiments were repeated 3 times; in each set of repetitions random blocks were chosen for analysis.

2.6. Cellular adhesion and migration assay

To investigate the ability of NCI-H460 cells to adhere to and migrate inserts containing porous membranes (8.0 μm pore size; Becton Dickinson) were used. Briefly, the porous membranes were hydrated in the cell culture media for 2 h at 37 °C and 5 % CO_2, then the inserts were placed in a 24 well plate containing 0.5 mL of RPMI media with 10 % FBS. Cells were suspended at a density of 1×10^5 cell/well in 0.5 mL of serum free media and seeded inside the inserts for 24 h. Non-migrated cells inside the inserts were removed with a wet cotton swab. The migrated cells on the underside of the inserts were stained and fixed by sequentially transferring the inserts through 3 solutions provided in a manufacturer kit (Diff-Quik fixative reagent, Diff-Quik solution I, and Diff-Quik solution II, Fisher) upon two water rinses in between. The cells' nuclei were stained purple (Diff-Quik Solution II) while cells' cytoplasms were stained pink (Diff-Quik Solution I). The cell culture inserts were then allowed to air dry upside down, overnight, and at room temperature. Images were obtained using a fluorescence microscope (Leica Microsystems; 10× objective). Experiment was repeated 3 times, and at least 10 random fields of view were inspected for each sample and in every trial, while counting all cells for each experiment.

2.7. Western blot analysis

NCI-H460 cells were seeded overnight in 6-well plates (Fisher) at a density of 5×10^5 cell/ well, and treated with digitoxin (10, 25, and 50 nM) or D6MA (1, 5, and 10 nM) for 24 h. Following exposure, the cells were lysed for 30 min in a lysis buffer containing 2 % Triton X-100 (Sigma), 1 % sodium dodecyl sulfate (SDS), 100 mM sodium chloride (NaCl), 10 mM tris-hydrochloric acid (HCl), complete mini cocktail protease inhibitors (all reagents are purchased from Roche) and 1 mM EDTA and centrifuged at 4 °C and 12,500 rpm for 15 min. The amount of proteins in the supernatant were determined using standard Bicinchoninic Acid Assay (BCA, Thermo Scientific). Briefly, working reagent was prepared according to the manufacturer instructions by mixing 50 parts of reagent A with 1 part of reagent B (reagents included with the kit). Two μL of each sample was added to a 96-well plate and incubated with 200 μL of the working reagent at 37 °C for 30 min. Control calibration curves were prepared using serial dilutions of standard bovine serum albumin (BSA). Absorbance at 562 nm was recorded via the FLOUstar OPTIMA plate reader.

Protein in lysed samples and standard protein ladder (Fisher Scientific) were separated by a 7.5 or 10% SDS–polyacrylamide gel electrophoresis (PAGE) gel and transferred to polyvinylidene fluoride (PVDF) membranes using a wet transfer method. Membranes were blocked in 5 % non-fat milk in distilled water for 2 h at room temperature, and subsequently incubated with the primary antibody at 4 °C overnight. The membranes were washed 3 times in Tris-buffered saline-Tween 20 (TBS-T; 25 mM Tris–HCl, and 125 mM NaCl, Sigma Chemicals, and 1% Tween 20, Fisher Scientific) for 10 min each, incubated with horseradish peroxidase-conjugated secondary antibody (Cell Signaling) for 1 h at room temperature, washed again (3 times for 10 min in TBS-T) and developed by chemiluminescence (Supersignal, ThermoFisher). Antibodies against integrin α4, matrix metalloproteinase-2 (MMP-2), matrix metalloproteinase-9 (MMP-9), extracellular signal-regulated kinase (ERK 1/2), phosphatidylinositol 3-kinase (PI3K), protein kinase B (AκT), and nuclear factor-kappa B (NF-κB) were investigated (Cell Signaling Technology). Band quantification was performed using ImageJ software, version 10.2. Experiments were performed in duplicates and repeated 3 times. Expressions levels in each sample were normalized against expression of control β-actin (Sigma).

2.8. Global genome expression analysis

NCI-H460 cells were seeded overnight in 60 mm^2 plates (Fisher) at a density of 1×10^6 cell/ plate. Subsequently, the cells were treated with digitoxin (10 and 25 nM), D6MA (1 and 5 nM), or DMSO vehicle control (< 0.1%) for 12 h; experiments were performed in triplicate. Global gene expression analysis of treated and control cells was performed using high-throughput mRNA microarray analysis. For this, mRNA was collected from each group using RNeasy Mini kits according to the manufacturer's protocol (Qiagen). Briefly, cells were lysed, mixed with 1 volume of 70% ethanol (Sigma), loaded onto spin column, centrifuged and washed repeatedly. RNA elution was collected using 40 μL of nuclease-free water. RNA quality was assessed using Eppendorf (BioPhotomer) set at 260/ 280 nm absorbance ratio. Upon collection, samples were stored at −80 °C and shipped to ArrayStar (Rockville, MD) for analysis.

Total RNA was quantified and assessed for quality with a NanoDrop ND-1000 and denaturing agarose gel electrophoresis. RNA was reverse transcribed to cDNA with a Superscript ds-cDNA kit (Invitrogen), labeled with one-color Cy3 DNA labeling (NimbleGen), hybridized to a NimbleGen 12x135k human gene microarray with 45,033 probes with an average of 3 probes per target gene. Array scans were performed by Axon GenePix 4000B microarray scanner (Molecular Devices). Images were imported to NimbleScan software (v2.5) for alignment and expression analysis. Expression data were normalized via quantile normalization and Robust Multichip Average algorithm to generate probe and gene level files for Agilent GeneSpring GX (v12) analysis. Genes with 5 out of 15 samples greater than the lower cutoff were chosen for analysis. Volcano plots with $p < .05$ (*t*-test) and 2-fold change in expression compared to DMSO control determined differentially expressed genes (DEGs).

DEGs were uploaded to Ingenuity Pathway Analysis (Qiagen) to conduct pathway analysis to thus evaluate the underlying signaling associated with the proposed hypothesis [25]. Only DEGs with known translated proteins were included. Briefly, core analysis was conducted to identify the top ranked biofunctions, canonical pathways, and disease functions associated with digitoxin and D6MA exposure to NSCLC cells. Z scores were used to predict activation or inhibition of those genes and functions up- and downstream of observed signaling respectively. Gene signaling networks were constructed and ranked based on likelihood of them not occurring by chance at $p < .05$. Signaling pathways/networks for functions of interest were plotted to evaluate underlying gene signaling to explain observed phenotypic behaviors.

2.9. Statistical analysis

Results are represented as mean ± standard deviation. Two-way analysis of variance (ANOVA) and unpaired two-tailed Student's *t*-test were performed using JMP 8.0 (SAS Institute) and SigmaPlot 10.0 (Systat Software Inc.) to compare across treatment groups (confirmed using t-test). The number of replicates for each experiment was detailed in their respective section. For all experiments, results are considered significant when $*p < .05$.

3. Results and discussion

The present study hypothesized that digitoxin, a cardiac glycoside (CG), and α digitoxigenin-α-L-rhamnoside (D6MA), a synthetic analog (Supporting Information Scheme 1) can reorganize malignant cell cytoskeleton and reduce their dynamics and migratory ability to thus eliminate their tumorigenicity. To demonstrate our hypothesis, the cellular systems used as models were non-small cell lung carcinoma cells (NSCLC) from epithelial tissue; the model was proposed as pertinent based on previous reports that showed that 80–85% of lung cancers originate in these cells [10] and that such cells are susceptible to our compounds [6,7,13]. Moreover, previous research has showed that these cells have increased resistance to chemotherapy [14] thus leading to poor clinical and therapeutic outcomes [29]. Complementary, the cellular models to represent a model of normal, non-cancerous lung epithelial cells were BEAS-2B cells [30].

3.1. Realtime monitoring of cellular behavior following exposure to digitoxin and D6MA

We first assessed cellular behavior upon exposure of the model cells to sub-therapeutic, therapeutic, and toxic concentrations of digitoxin (10, 25, 50, and 100 nM, respectively) and their therapeutic concentrations of D6MA (1, 5, 10, and 25 nM), in real-time. The assessment was based on electric cell impedance sensing (ECIS) which was previously shown to allow for evaluation of cell proliferation [31], morphology [31,32], and adherence [31,32,33], all considering the insulating nature of the cellular membrane which causes measurable changes in cellular resistance [31,32,33] onto gold electrodes [34,35]. ECIS usage was also aimed to help discriminate possible selectivity of digitoxin and D6MA toward cancerous lung cells [7], as well as to identify the therapeutic window for such compounds, all in a high-throughput manner [36,37,31].

For the experiments, 24 h prior to digitoxin and D6MA exposure, cells were immobilized onto the ECIS gold electrodes and allowed to attach, spread, and grow until the complete formation of a cell monolayer (as indicated by a settlement in the resistance value; Supplementary Fig. S1). Attached cells were subsequently treated with sub-therapeutic, therapeutic, and toxic concentrations of digitoxin (10, 25, 50, and 100 nM) and their equivalent concentrations of D6MA (1, 5, 10, and 25 nM respectively); herein the sub-therapeutic, therapeutic, and toxic concentrations were defined based on their effect on cellular proliferation/ viability as shown by previous studies [6,7,38]. Specifically, therapeutic and toxic doses (50 and 100 nM for digitoxin and 10 and 25 nM for D6MA, respectively) were previously shown to cause a decrease in cellular proliferation and cell viability, whereas sub-therapeutic concentrations caused for changes in cellular adhesion [13]. Additionally, our previous analyses have showed that the concentrations of D6MA to produce apoptosis or cell cycle arrest in NCI-H460 cells were on average 4 to 10 times lower than the concentrations of digitoxin that were to produce the same effects [6,7].

Fig. 1a and b show changes in NCI-H460 cells behavior upon exposure of such cells to different concentrations of digitoxin and D6MA, respectively. Specifically, analysis showed both time and dose dependent changes, with the resistance values of the cells treated with lower concentrations of both compounds (10 and 25 nM for digitoxin, and 1 and 5 nM for D6MA respectively) being steadily higher than the resistance values of the control cells (i.e., cells not treated with the compounds). Furthermore, the resistance values for cells treated with 25 nM digitoxin were higher than those for cells treated with 10 nM digitoxin. Contrary, the resistance values for cells treated with 5 nM D6MA were higher than the values for 1 nM treated cells and the controls, until around 24 and 42 h post exposure, respectively. Such trend subsequently dropped to lower resistance values than those recorded for 1 nM treated cells and the control cells, respectively. Moreover, the resistance values for cells treated with the higher concentrations of both drugs (50 and 100 nM digitoxin and 10 and 25 nM D6MA, respectively) underwent drastic changes when compared to the resistance values for the control cells or cells treated with lower concentrations of these compounds. Specifically, after an initial increase, a sharp drop was recorded around 5 h for the cells treated with concentrations of 100 nM digitoxin and 25 nM D6MA, and around 8 h for cells treated with 50 nM digitoxin and 10 nM D6MA, respectively.

Fig. 1c and d showed for the first time the high-throughput and real-time screening analysis of the normalized resistance values associated with the behavior of control BEAS-2B cells upon their exposure to similar concentrations of both compounds. Results indicated that exposure to high and low concentrations of digitoxin and D6MA did not lead to any major changes in cellular resistance when compared to the resistance of controls (i.e., not treated cells), with such results confirming previous studies reporting on compounds' selectivity toward neoplastic cells compared to normal cells [6].

The recorded drop in the resistance values is presumably associated with the compounds ability to induce apoptosis and reduce cellular viability at the tested concentrations [39,40], presumably indicating activation of different signaling pathways that led to distinct cellular behavior and fate of the treated group [41,42]. Specifically, analysis showed that the percentage of apoptotic cells increased in a dose-dependent manner when NCI-H460 cells were treated with digitoxin or D6MA (Supplementary Fig. S2). Similarly, the number of live cells decreased in a dose-dependent manner for NCI-H460 cells treated with digitoxin or D6MA (Supplementary Fig. S3). Furthermore, exposure to 100 nM digitoxin and 25 nM D6MA significantly reduced cellular viability by more than 90 %.

Overall, the differences in the resistance values between cells treated with both compounds and across the different concentrations of the compounds being tested, suggested the existence of a threshold concentration that would eventually lead to distinct cellular behavior and fate. This was further confirmed when changes in cell-adhesion properties were investigated through the use of the ECIS platform. Briefly, previous analysis showed that ECIS allows for evaluation of the alpha parameter to reflect the restrictions on the AC current passing underneath immobilized cells, with such parameter to be used to establish a direct relationship of cell adhesion strengths profile [13]. In particular, an increase in alpha indicated a decrease in the distance between the cell and the electrode itself thus suggesting an increase in the cellular adhesion properties [32,13,43].

Our analysis (Fig. 2) showed that the alpha parameter followed a similar trend as the resistance one, with minor differences being observed across the corresponding concentrations of both compounds being tested. Specifically, while exposure to the low concentrations of digitoxin (10 and 25 nM) and D6MA (1 and 5 nM) resulted in an increase in alpha for the NCI-H460 cells, with such increase persisting over time, exposure to the high concentration of both compounds (i.e., for digitoxin 50 and 100 nM, and for D6MA 10 and 25 nM, respectively) resulted in an increase only within the first hours of exposure. This was followed by a sharp drop, all in a dose-dependent manner. Since the dose ranges of both compounds showed minimal effect on BEAS-2B cells in Fig. 1 and in our previous work [6,7,13], only alpha parameter values of NCI-H460 cells were evaluated.

Cross comparison in the normalized alpha parameter of treated cells relative to control cells indicated that exposure to 10 and 25 nM

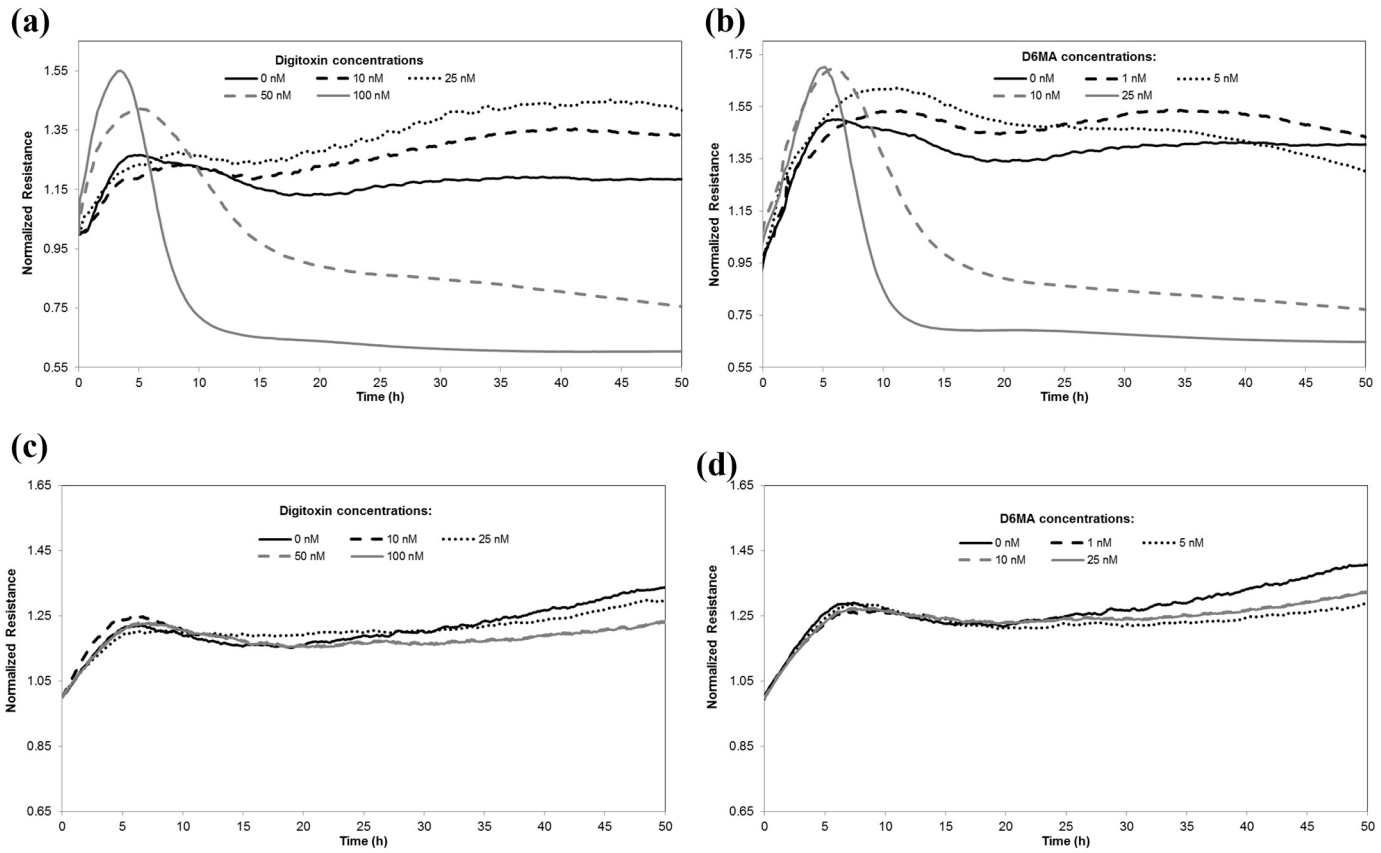

Fig. 1. Representative normalized resistance values of NCI-H460 cells upon exposure to different concentrations of (a) digitoxin and (b) D6MA. Representative normalized resistance values of BEAS-2B cells upon exposure to different concentrations of (c) digitoxin and (d) D6MA. The cellular resistance values were recorded every 12 min for up to 50 h post treatment ($n = 8$).

digitoxin and 1 and 5 nM D6MA respectively, resulted in an approximate average increase of 10–15 and 12–20 % after 24 and 48 h respectively. In contrast, exposure to high concentrations resulted in a time, dose, and compound dependent alpha decrease, where exposure to 50 nM digitoxin led to 21 and 37 % decrease, and exposure to 10 nM D6MA led to 43 and 60 % decrease, both when compared to control cells after 24 and 48 h, respectively. Similarly, a 73 and 90 %, and 80 and 95 % decrease in the alpha parameters was observed when cells were treated with 100 nM digitoxin and 25 nM D6MA after 24 and 48 h, respectively.

The increase in alpha recorded at low treatment concentrations suggests that both digitoxin and D6MA promote cellular adhesion and thus hints at a less migratory behavior of such cells to potentially resemble non-metastatic cell lines [44,45]. Contrary, the decrease in alpha observed upon cellular treatment with high concentrations of compounds is correlated to increased compound ability to induce apoptosis and lower cellular viability [6] thus supporting a loss of cellular adhesion and overall integrity of the cell monolayer [46].

3.2. Effects of digitoxin and D6MA on cellular migration

Considering the above ECIS analyses showing changes in cell adhesion, we further investigated whether such changes are influencing the ability of the treated cells to migrate. For this, the NCI-H460 cells were treated with either of the compounds for 24 h, counted and subsequently such live cells were used in equal amounts and immobilized onto porous membranes for cell migration assay [28,27,26,25]. Previous analyses have showed that cell deformation [47,48] and loss of focal adhesion lead to increased cell motility [48,49], with Gamal et al., showing that higher migration rates were associated with cells with relatively lower adhesion values [50].

Fig. 3a and b display optical images and quantification of the NCI-H460 migration abilities upon treatment with both compounds. Overall, both compounds showed a decrease in migration presumably due to induced changes in cytoskeleton or cytoskeleton-induced cellular signaling. This hypothesis is supported by previous studies that showed that the cytoskeleton components can act as both receptors and targets in different cellular pathways [51,52]. While there were no differences observed between the corresponding concentrations of the compounds, there were however significant differences being observed between treatment with therapeutic and sub-therapeutic concentrations of both compounds. Specifically, exposure to 10, 25, and 50 nM digitoxin resulted in 25, 40, and 63 % significant reductions in the number of migrated cells relative to migration of control cells. Similarly, cells treated with 1, 5 and 10 nM D6MA resulted in 13, 44, and 79 % significant reduction in the number of migrated cells, again, relative to control cells.

3.3. Effects of digitoxin and D6MA exposure on cellular size and elasticity

Changes in cytoskeleton were confirmed using cell size analysis; specifically, the volume of the cells after 24 h of exposure to both digitoxin (10, 25, and 50 nM) and D6MA (1, 5, and 10 nM) was investigated using fluorescent assisted cell sorting (FACS) and comparing the side and forward scatter of the suspended cells to calibration beads used as controls [36]. The use of calibration beads and forwards and side scatter plots respectively also provided a viable way to detect the phenotype of cells and their abundance [53], thus allowing for overall information on their physiological states [54] and height evaluations [55]. For these analyses we did not consider exposure to 100 nM digitoxin and 25 nM D6MA, respectively, due to the large reductions observed in cellular viability and summarized in Supplementary Figs.

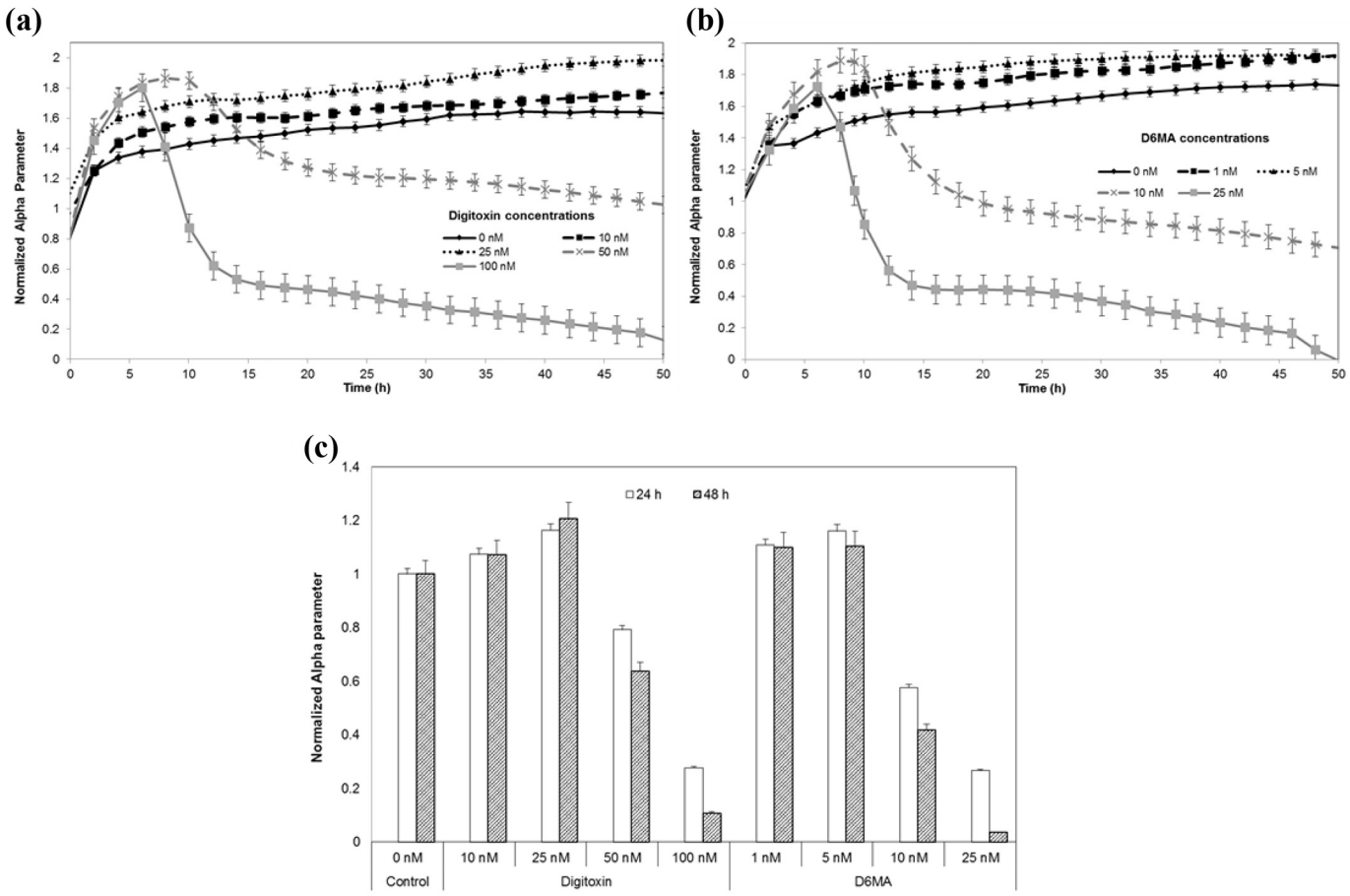

Fig. 2. Representative normalized alpha parameter following NCI-H460 cells exposure to (a) digitoxin and (b) D6MA. (c) Cross comparison of the normalized alpha value for cells treated with digitoxin and D6MA after 24 and 48 h respectively. Analysis of the alpha parameter were recorded every 12 min (n = 8).

S2 and S3, respectively.

Fig. 4a shows that the average volume for all cells treated with different concentrations of digitoxin and D6MA significantly increased by approximately 5–7% when compared to control cells. No significant differences were however observed among the different doses or the compounds themselves.

Secondly, cellular elasticity was investigated for confirming changes in treated cells' cytoskeleton. Previous reports showed that changes in ECIS recorded resistance as resulted from the changes in cell morphology, size, adhesion, and migration are likely due to cytoskeletal alterations [31,56] which can lead to changes in cellular elasticity [57,58,59] and rigidity [47], respectively. Our analysis using atomic force microscopy (AFM) tapping mode following 24 h exposure of NCI-H460 cells to both compounds showed that the average cellular Young's modulus dropped by 20 % for cells treated with 10 nM digitoxin, 55 % for cells treated with 25 nM digitoxin, and 63 % for cells treated with 50 nM digitoxin, all relative to the control cells (Fig. 4B). Contrary, the cellular elasticity for cells treated with 1 and 5 nM D6MA showed a 22 and 41 % increase in Young's elastic modulus relative to control cells, which was significantly higher than the elasticity of the cells treated with digitoxin at the corresponding doses. Cells treated with 10 nM D6MA showed a 90 % decrease in the cellular elasticity when compared to control cells, which was also significantly lower relative to the D6MA's other two lower doses being tested.

The significant alterations in Young's modulus confirmed alterations to the cellular cytoskeleton [57,58] to support our above reported differences in resistance, adhesion, and cell volume. Further, the lower values of Young's modulus displayed by NCI-H460 cells treated with digitoxin and 10 nM D6MA, relative to the control cells respectively, might indicate that an individual cell gains the ability to deform [57] and potentially increase its motility [60]. Cells treated with 1 and 5 nM D6MA showed a more rigid behavior relative to control cells, presumably reflecting their decreased ability to deform [61,57,62], as well as favoring a higher adhesion, as supported by our analysis of alpha parameter.

3.4. Effects of digitoxin and D6MA on the expression of cellular regulatory proteins

Considering the observed changes in cell adhesion, migration, and elasticity, the expression levels of matrix metalloproteinases (MMPs; i.e., MMP-2 and MMP-9) and integrin α4 were also investigated. Previous analysis showed that MMPs are a family of proteinases involved in the proteolytic degradation of the extracellular matrix (ECM) [63,64,65] and known to play major roles in cellular migration, tumor growth, and metastasis [63,64,66]. Furthermore, previous analyses showed that MMP-2 contributes to cancer cell migration [63,67,68] through its role as a key enzyme in metastasis [67,68], while MMP-9 mostly mediates cell migration [69,70,71]. Additionally, previous studies revealed that both MMP-2 and MMP-9 can be secreted in active forms to degrade ECM specific macromolecules and to facilitate cancer progression through their involvement with MMP-14 as well as through their overall participation in tumor angiogenesis [63]. Lastly, reports also showed that overexpression of both MMP-2 and MMP-9 was associated with epithelial to mesenchymal transition (EMT) [63] while studies on integrin α4 were shown that the proteins has an active role in increased cell migration and reduces cell spreading by focal adhesion formation relative to other β_1 integrins for instance [72], with Kassner

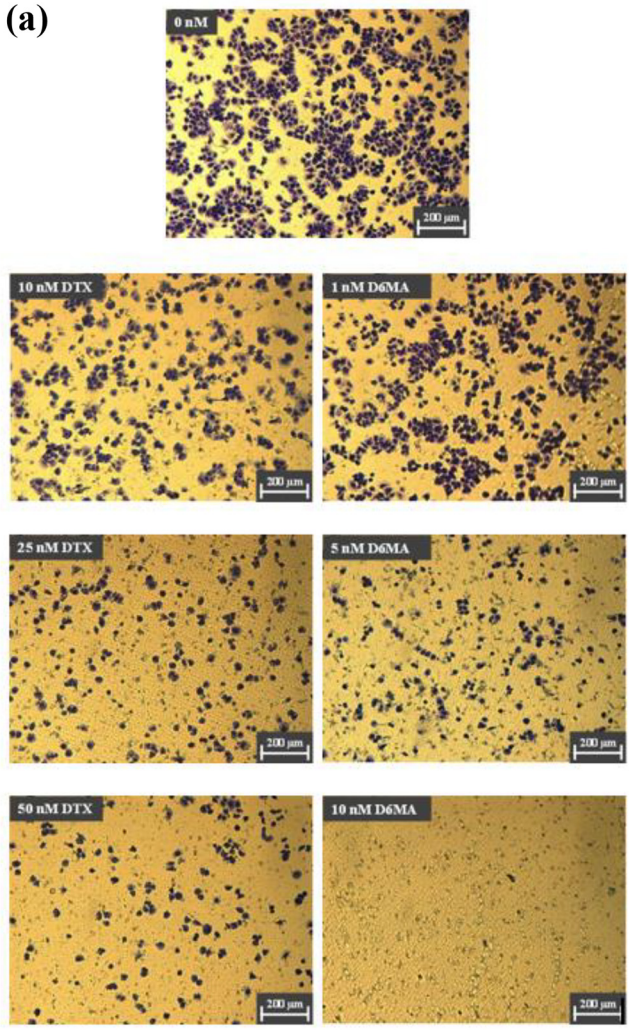

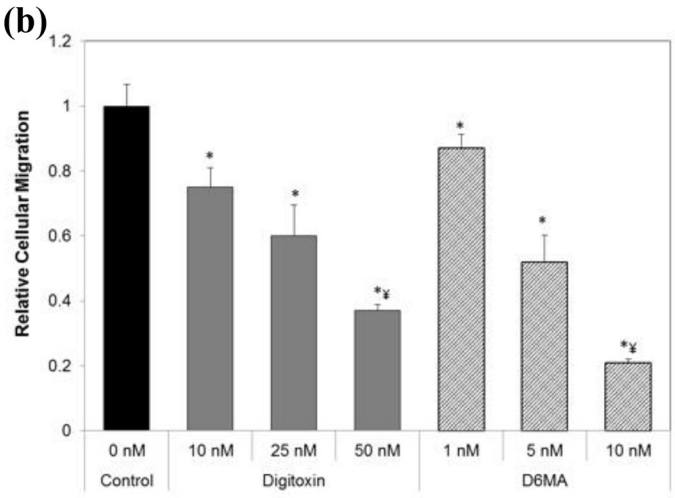

Fig. 3. (a) Optical images of cellular migration abilities of controls and NCI-H460 cells treated for 24 h to different compounds. (b) Quantification of NCI-H460 cellular migration capabilities following 24 h exposure to different concentrations of digitoxin and D6MA. The symbol * indicates a significant difference from the control ($p < .05$), with the symbol ¥ indicating a significant difference between the exposure doses (both therapeutic and sub-therapeutic ones).

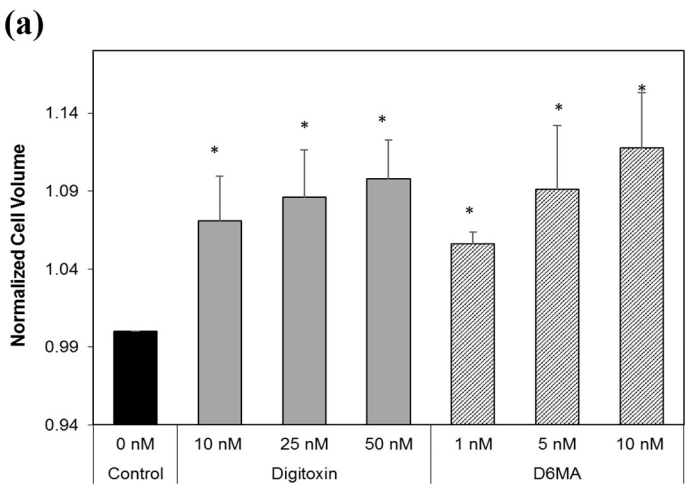

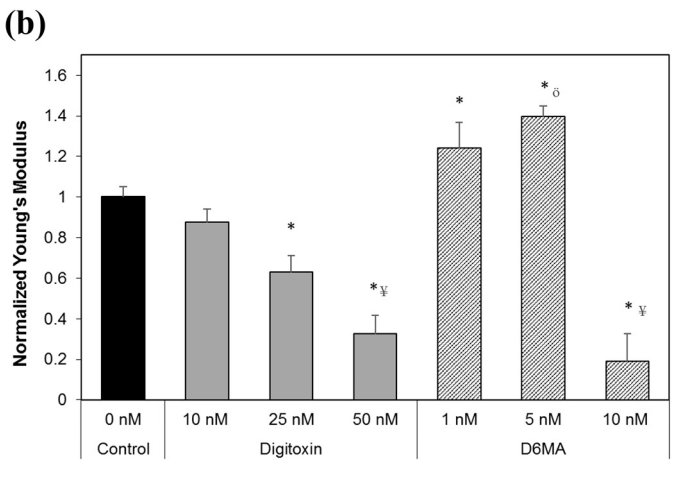

Fig. 4. (a) Overall volume of NCI-H460 cells following 24 h treatment with different concentrations of digitoxin and D6MA. (b) Young's modulus analysis. The symbol * indicates a significant difference from the control ($p < .05$, $n = 3$), the symbol ö indicates a significant difference between drugs, and the symbol ¥ indicates a significant difference between therapeutic and sub-therapeutic doses.

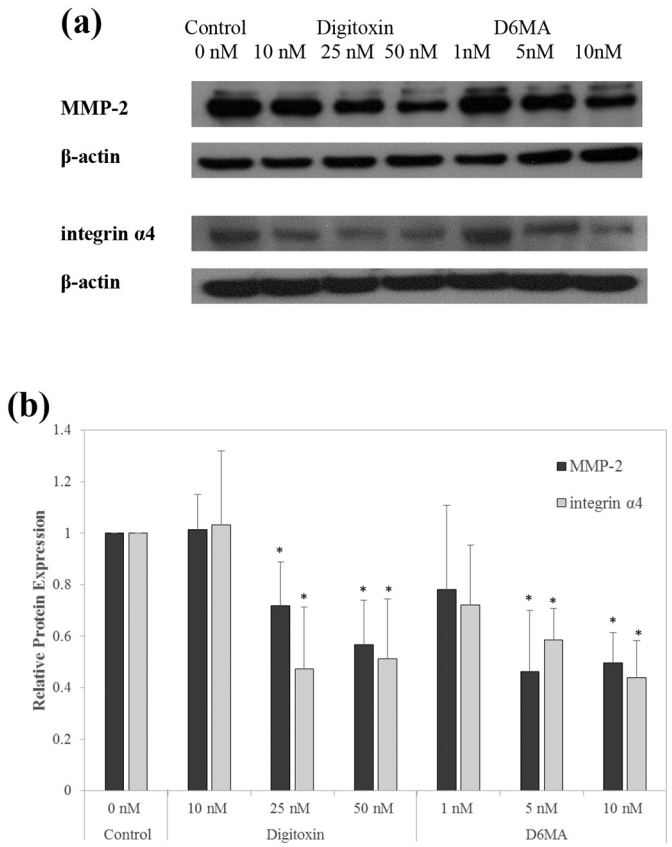

Fig. 5. Western blot analyses of (a) MMP-2 and integrin α4, along with (b) quantification after 24 h exposure of NCI-H460 cells to varying concentrations of digitoxin and D6MA. The symbol * indicates a significant difference from the control ($p < .05$).

et al., demonstrating that integrin's α4 tail largely promotes cellular migration [73].

Our analysis showed that both digitoxin and D6MA caused significant decreases in the expression of the MMPs (Fig. 5 and Supplementary Fig. S4) at 24 h post treatment. Specifically, the expression of MMP-2 decreased in a dose dependent manner upon treatment with digitoxin, with exposure to 25 and 50 nM causing 28 and 43% decrease relative to control cells. Exposure to 5 and 10 nM D6MA also caused significant decreases in the expression of MMP-2 by 54 and 50 %, respectively, again, relative to control cells. All doses of digitoxin and D6MA showed decreases in the expression of MMP-9 relative to the control cells; however only 10 and 50 nM digitoxin and 1 and 5 nM D6MA respectively, caused significant decreases relative to controls. Furthermore, treatment with 10, 25, and 50 nM digitoxin resulted in 42, 32, and 54 % reductions while exposures to 1, 5, and 10 nM D6MA resulted in 32, 23, and 38 % reductions in MMP-9 expression. There were no significant differences in the two MMPs expression levels between the two compounds and their corresponding doses respectively.

Treatment with both digitoxin and D6MA also caused significant decreases in the expression of integrin α4 (Fig. 5) at 24 h post-treatment. Specifically, cells treated with 25 and 50 nM digitoxin displayed significant 53 and 49 % decreases in integrin α4 relative to the control cells respectively. Cells treated with all three doses of D6MA displayed decreases in the expression levels of integrin α4, but only the doses of 5 and 10 nM showed that such decreases were significant when compared to the controls. Furthermore, D6MA also caused a dose-dependent response with exposure to 1, 5, and 10 nM causing reductions in integrin α4 expression of 28, 41, and 56 %, all relative to the controls. Similar to the MMP expression, there were no significant differences in the integrin α4 expression levels between the two compounds and their corresponding doses respectively.

The decreased MMP expression further confirmed decreased migratory abilities of treated cells, presumably indicating that integrin α4 might play a potential role in cell stabilization. Such a hypothesis is supported by previous research that showed that the expression of integrins correlates to the activation of MMPs [64,74,75,76,77] with the interaction between integrins and MMPs being previously demonstrated to play a key role in cellular invasion process [78] when considering their roles as substrates for MMPs [63,78].

3.5. Global genome expression analysis

Genome expression signaling analysis found that both compounds significantly inhibited cancer, cancer-associated respiratory disease, and malignant reproductive disease signaling ($Z < -2$) at 12 h post-treatment. Several dose-dependent changes in NCI-H460 cells following treatment with each compound were identified and were both compound and dose dependent. Specifically, 10 nM digitoxin caused 209 differentially expressed genes (DEGs), with predicted activation of cell signaling, immune cell trafficking, recruitment, and movement, with an inhibition prediction of cell proliferation and colony formation respectively (Fig. 6a). Additional functions that were significantly influenced included cell morphology, organization, development, and maintenance.

The higher dose of 25 nM digitoxin caused 769 DEGs with predicted inhibition of cell development, morphology, and proliferation, thus further reinforcing activation of cell death, muscle differentiation, and shape change of treated cells. Of note, inhibited cell development included inhibition of hyperplasia, epithelial neoplasia, lung carcinoma, lung tumor, and several leukemias. Cell movement, signaling, morphology, and organization were also significantly impacted. Conversely, equipotent concentration of 1 nM D6MA to 10 nM digitoxin caused 1496 DEGs with predicted activation of cell movement, cytoskeleton assembly/organization, maintenance, morphology, and skeletal and connective tissue development. Inhibited functions included cell survival. Moreover, 5 nM D6MA exposure caused 1636 DEGs with predicted activation of cell death, apoptosis, and necrosis through inhibition of epithelial cell quantity, proliferation, membrane formation, plasma membrane projections, and cell activation. Similar to 25 nM digitoxin, colony formation, lung tumor, and adenoma development functions were also inhibited.

To further evaluate both upstream and downstream signaling pathways associated with the above behavior and concrete protein expression responses, ranked canonical pathway and network analyses were screened. Based on behavioral and initial core analysis findings, our detailed evaluation was restricted to 25 nM digitoxin and 5 nM D6MA. For 25 nM digitoxin, the highest ranked network had MMP2, activated focal adhesion kinase, PLAU, OSM, and Ap1 complex associated with cardiac disease and organismal injury and abnormalities. The 4th highest ranked network showed predicted inhibition of NF-κB complex as a hub gene for signaling as associated with cell morphology, humoral response, and protein synthesis (Fig. 6b). In addition, the 5th highest ranked network showed hub genes down-regulated phosphatidylinositol 3-kinase (PI3K) family (PIK3C2B), an upstream effector on protein kinase B (AκT) with known wortmannin sensitivity [79], as well as MMP14 associated with cell movement, connective tissue disorder, and dermatological disease. Down-regulation of BCL2, an anti-apoptotic gene typically over-expressed in cancer cells, lent further evidence to reduced AκT signaling.

Enhanced invasion signaling was noted in the actin cytoskeleton signaling pathway primarily associated with over-expressed ITGA3 and ITGB4, receptors for ECM proteins and MMP over-expression. However, a 105-fold downregulation of fibronectin (FN1) suggested that over-expression of integrin mRNA may be a response to reduced ECM matrix synthesis and reduced ability of NCI-H460 to adhere to the extracellular environment, thus confirming both our alpha and elasticity analysis.

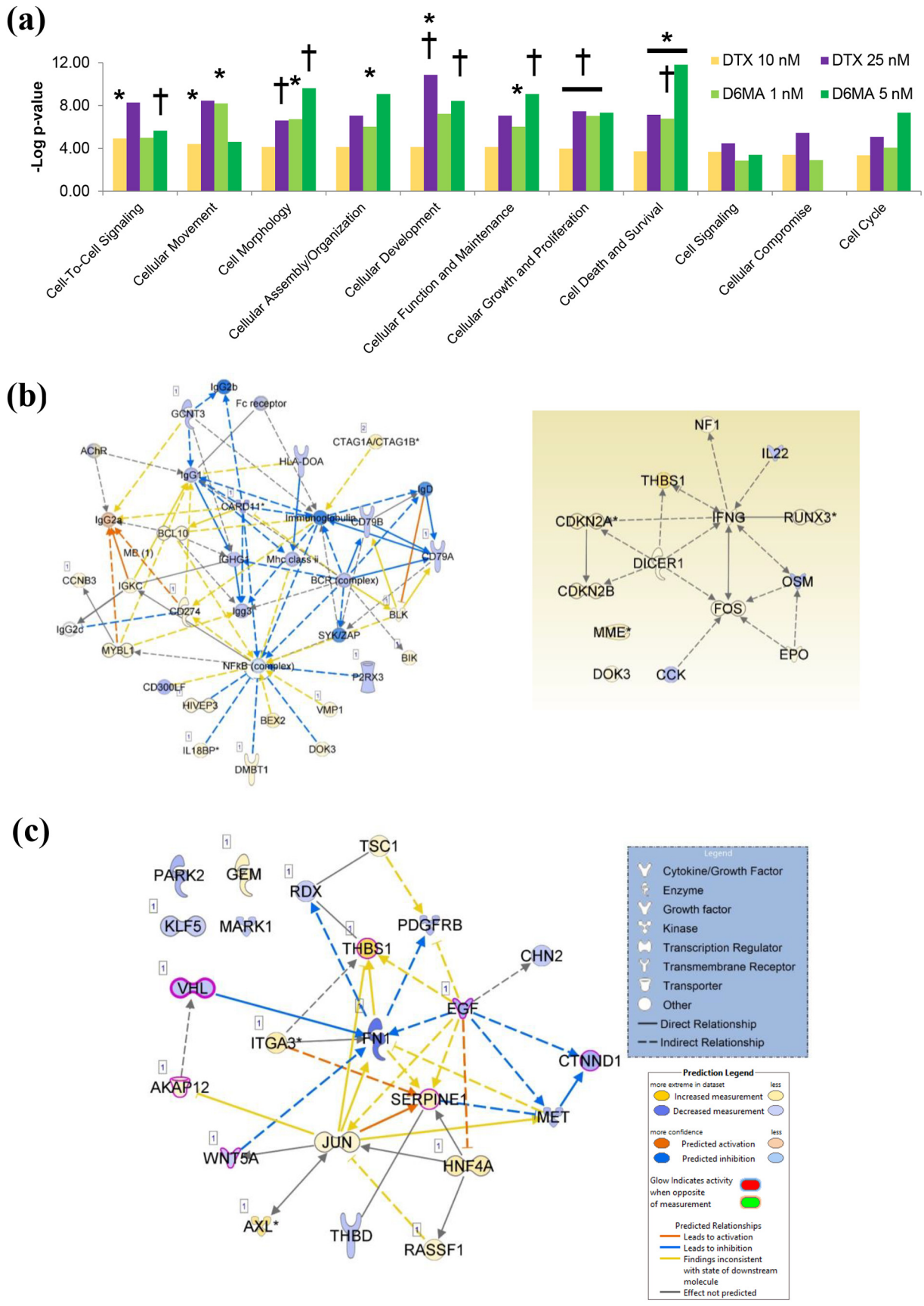

Fig. 6. Global genome analysis of digitoxin- and D6MA-treated NCI-H460 reveals major changes to anti-lung cancer signaling. a) Dose-dependent altered cell functions upon digitoxin and D6MA at 12 h post-treatment. Symbols * and † indicate predicted activation and inhibition, respectively ($Z \geq \pm 2$). b) Inhibition of NF-κB signaling (left) and epithelial tumor inhibition signaling (right) following 25 nM digitoxin exposure. c) Inhibition of lung tumor network associated with altered microtubule dynamics following cellular treatment with 5 nM D6MA.

Furthermore, NF-κB downregulation could inhibit MMP expression. By 24 h post-treatment, decreased α4 expression suggested the potential for decreased cellular ability and adherence to ECM. Over-expression of myosin genes along with inactivation of PI3K, RAC, CFL, and F-actin polymerization suggested actin cytoskeleton instability and cytoskeleton reorganization, similar to D6-MA (see below).

For 5 nM D6MA, several similarities in intracellular signaling were evident, including over-expressed FOS, CDKN2A, THBS1, as well as down-regulated FN1 that were associated with cell compromise, cell cycle, and cell signaling functions. Unique anti-cancer function signaling was associated with hub genes over-expressed MDM2, NRG family, HNF4A and under-expressed ALDH family, SOS1, KRAS, POT1, RIF1, in the top ranked networks associated with p53, actin cytoskeleton, telomere, development and cell cycle functions. In addition to these genes, examination of top-ranked canonical networks indicated several over-expressed MMPs, ATM, several Erk/ Jnk protein kinases in several cancer pathways, and decreased EGF and MET in bladder cancer and micropinocytosis pathways.

To investigate how changes in cell morphology, actin cytoskeleton, and focal adhesion signaling relate to inhibition of epithelial neoplasia and tumors, lung cancer inhibition and lung neoplasia inhibition networks respectively were also plotted for 25 nM digitoxin-treated NCI-H460. Subsequently, genes associated with cell morphology were identified. Hub genes of these large networks were similar and included over-expressed INFG, DICER1, CDKN2A, ITGA3, MMP14, and down-regulated BCL2, FN1, LEP, ITGAX, C3, and F2 respectively; 34 out of 154 genes were associated with morphology, actin cytoskeleton, and adhesion (Supplementary Fig. S5a).

To simplify this network, we also filtered the gene expressions that were only associated with inhibition of epithelial tumors. The resulting small signaling network included genes taking key roles in the highest ranked signaling networks (Fig. 6b, right). Over-expressed interferon gamma (IFNG), DICER1, FOS, RUNX3, and CDKN2A/B (p16/p15) were present. INFG has been previously shown to play important immunoregulatory and anti-proliferative functions on transformed cells [80].

Our finding agrees with a previous study reporting that interferons regulate protein/protein interactions following digitoxin exposures in pancreatic cancer cells [81]. CGs along with increased interferon gamma may synergistically act on differentiating cancer cells to earlier, more benign phenotypes, including moving leukemia cells to pre-macrophage/monocyte phenotype [82]. DICER1, a key enzyme in miRNA processing, RUNX3, and CDKN2A/B tumor suppressor over-expression possess roles in slowing cancer cell proliferation, differentiates NCI-H460 toward a more epithelial phenotype, and drastically improving patient survival. Such finding correlates well with our previous publications showing S and G2 cell cycle arrest at therapeutic digitoxin concentrations [6,83,84]. Chen et al. [85] reported that (+) strebloside, a natural monosaccharide tree extract, caused G2 cell cycle arrest and decreased NF-κB expression via Na^+/K^+-ATPase in ovarian cancer cell lines, however, exhibited equivalent or worse potency when compared to digitoxin. Downstream targets with anti-cancer activities included over-expressed NF1, FOS, and THBS1, which are associated with Ras pathway inhibition, cell differentiation, Na^+/K^+-ATP-ase-mediated pro-apoptotic regulatory ability, angiogenesis inhibition, and pro-adhesive ability in lung cancer cells [86–88].

For 5 nM D6MA, examination of the 400 gene inhibition of lung tumor signaling network revealed several cell's structure and morphology-associated signaling changes contributing to this network, including microtubule dynamics, actin cytoskeleton, inhibition of membrane projections, and tumor cell shape change respectively. In particular, actin cytoskeleton signaling in D6MA-treated NCI-H460 cells showed similar but more active effects when compared to digitoxin, with inhibition of ROCK pathways, increased RAC signaling, and decreased PAK1 and PAK3 expression resulting in increased focal adhesion, cytoskeleton reorganization, myosin light chain subunits, and inhibited actin polymerization respectively (Supplemental Fig. S5b).

Microtubule dynamics signaling was prevalent in both the epithelial neoplasia and inhibition of lung tumor signaling network. Gene expression was filtered for those genes that either affected or decreased lung cancer (Fig. 6c). This signaling network possessed over-expressed hub genes JUN, HNF4A, THBS1, and SERPINE1, with under expressed hub genes FN1 and EGF. Genes associated with an anti-tumor function included over-expressed THBS1 and AKAP12, with under-expressed EGF, CTNND1, WNT5A, and VHL. Such signaling suggested cytoskeleton alterations associated with anti-angiogenesis, anti-metastatic, anti-growth, and decreased WNT signaling [87,89–91].

3.6. Proposed molecular pathway to support cell transformation through reorganization of the cell cytoskeleton and reduction in its migration capabilities

Considering all the above results as well as previously published literature showing that different pathways associated with the mediation of MMPs' production via integrins are cell type dependent [92], we hypothesize that digitoxin and D6MA induce cytoskeleton reorganization and reduced motility via the PI3K/AκT pathway. These are further supported by previous studies that showed that PI3K/AκT pathway is implicated in cell migration and invasion as well as regulation of the transcriptional activity of NF-κB [93,94], which has binding sites on both MMP-2 and MMP-9 [94,95].

Indeed, our analysis support the hypothesis and showed that all three proteins associated with this pathway (namely PI3K, AκT, and NF-κB) were significantly affected upon cellular exposure to digitoxin and D6MA, though there were no significant differences between the corresponding doses of the two compounds at 24 h post-treatment (Fig. 7). Specifically, a significant decrease in PI3K was observed upon exposure of NCI-H460 cells to 10 and 50 nM digitoxin, with decreases in expression to 37 and 71 %, respectively. Further, all the doses of D6MA caused significant decreases in PI3K expression in a dose dependent manner, with 1, 5, and 10 nM causing decreases of 49, 64, and 75 %, respectively. Cardiac glycosides are known to bind to the plasma membrane-bound Na^+/K^+-ATPase to enact dose-dependent downstream signaling pathways. Exposure at or below therapeutic concentrations does not block Na^+/K^+-ATPase function, rather, the enzyme acts as a 'signalosome' to affect downstream pathways, including the PI3K-mediated inhibition of Aκt phosphorylation and decreased NF-κB activation [7,12,96]. Our findings suggest digitoxin and D6MA bind to and activate the Na^+/K^+-ATPase signalosome to affect both PI3K/Aκt and NF-κB signaling pathways.

The expression of AκT also decreased upon exposure to digitoxin and D6MA, but only at the highest dose for each compound, with 50 nM digitoxin causing for instance a reduction of 37 % and 10 nM D6MA causing a reduction of 35% respectively. The decrease in AκT expression appeared to occur in a dose dependent manner for both compounds. Finally, upon exposure to digitoxin, the expression of NF-κB decreased in a dose dependent manner with 0, 25, and 50 % reductions for 10, 25, and 50 nM digitoxin, respectively. However, only the 50 nM caused a significant effect relative to controls. A similar response was obtained for cells treated with D6MA, with decreases in expression of 7, 28, and 45 % for the doses of 1, 5, and 10 nM, respectively. NF-κB signaling is known to be influenced by cell shape, cell-to-cell contacts, and RhoA/ROCK/myosin signaling, with lower NF-κB signaling correlating with a more epithelial-like phenotype [97]. Our results correlate to these previous findings. Furthermore, global genome expression analysis revealed changes in cytoskeleton structure and maintenance, mainly associated with focal adhesion, Rac, and Pak family kinase signaling pathways; the changes clearly impacted NCI-H460 cell morphology leading to a loss in cell structure, increased adhesion, and thus loss of mobility. Upstream changes in Rac signaling are known to impact PAK signaling, which can influence downstream pathways of PI3K/AκT [98] currently explored as an emerging research area in Ras-driven cancers [99,100]. Inhibition of PAK signaling can halt

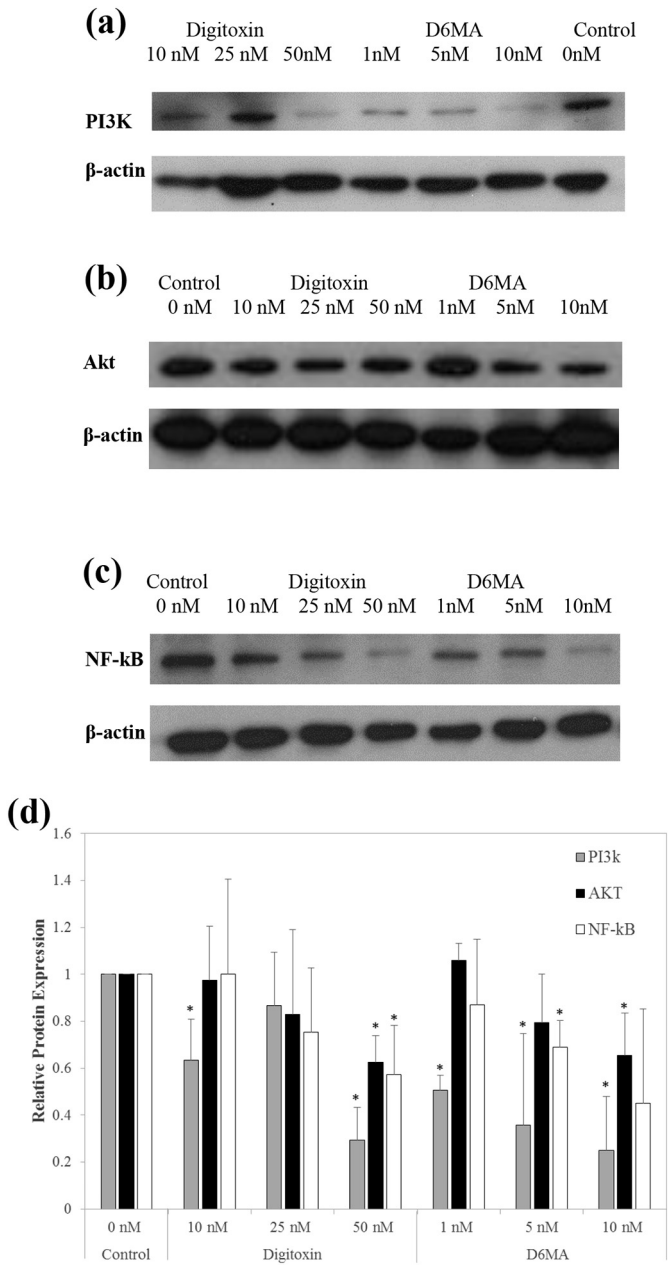

Fig. 7. Western blot analyses of (a) PI3K, (b) AκT, and (c) NF-κB along with (d) quantification after treatment for 24 h of NCI-H460 cells to digitoxin and D6MA. The symbol * indicates significant difference from the control ($p < .05$).

carcinogenesis progression, alter cell-to-cell signaling, and reverse EMT [101]. The culmination of these structural, morphological, and adhesion-related changes were clearly present in both digitoxin and D6MA anti-lung cancer signaling pathways presented herein.

Our conclusion of cytoskeleton reorganization and reduced migratory ability via the PI3K/AκT pathway is also supported by previous research by Chiu et al., that showed that the anticancer activity of *H. sabdariffa* leaf extract (HLE) for instance was through the AκT/NF-κB/MMP-9 cascade pathway, with HLE causing inhibition of MMP-9 expression due to inactivation of NF-κB as induced by a sustained inactivation of PI3K/AκT [93]. Further, studies by Wu et al., showed that the migratory abilities of hepatocellular carcinoma cells were reduced upon exposure to sinulariolide, a cembranolide obtained from the soft coral, in a concentration-dependent manner and again, due to suppression of the PI3K/AκT pathway and induced inhibition of MMP-2 and-9 activities [102].

Our findings also seem to indicate that digitoxin and D6MA appear to have the same mechanism of action, as similar trends and % reductions in viable expressed proteins were observed for the cells treated with the two compounds. The decreased expression of integrin α4 and MMPs, along with the suppression of the PI3K/AκT pathway at 24 h post-treatment did appear to depend on dose though, with all significant effects generally occurring at 25 and 50 nM digitoxin and 5 and 10 nM D6MA. Additionally, the anticancer effects of the high doses for both drugs (50 nM for digitoxin and 10 nM for D6MA) were likely occurring both via decreases in MMPs, leading to a decrease in cellular migration as well as by induced cell apoptosis. This effect was also observed by Wu et al., when sinulariolide was inducing hepatocarcinoma cell apoptosis while also inhibiting metastasis [102].

Our results thus increase the existing body of evidence associated with active mechanisms of anticancer activity for digitoxin [2,6,13], with such activity being attributed to transcriptional regulatory cascades associated with the Na^+/K^+-ATPase signalosome [6,7], inhibition of genes associated with cell proliferation, cell cycle arrest [6] and increases in adhesion due to enhanced CDK4/ZONAB/ZO-1 signaling [13], further adding the role of MMP into reprograming the NCI-H460 cells to presumably display a more benign phenotype via decreases in protein expression and inhibition of the resulting PI3K/AκT pathway. Our analysis ultimately showed decreased migratory abilities and stronger adhesion characteristics, similar to that of epithelial cells. These current findings along with current literature base were further supported by our global gene profiling analysis that predicted inhibition of NSCLC cell proliferation, epithelial neoplasia, and tumor growth. Collectively, these multi-target analysis and downstream effects would drastically impact the ability of a lung tumor to proliferate, thus suggesting the potential of digitoxin monosaccharide analog derivates as potential future chemotherapeutic agents.

4. Conclusions

We demonstrated the antitumor ability of digitoxin and its synthetic analog, D6MA, to cause cytoskeleton reorganization, increase adhesion, altered elasticity and reduced mobility in human non-small cancer lung (NCI-H460) cells. Specifically, our results first showed a selectivity of digitoxin and D6MA toward NCI-H460 cells over non-tumorigenic human lung epithelial cells (BEAS-2B), with D6MA having around a 5x more potent effect, as confirmed both through single point and high-throughput real-time assays. Next, exposure to the compounds caused for increases in cell adhesion, changes in cellular volume and elasticity, and decreases in their migratory abilities. Such effects appear to be caused by a decreased expression of MMPs regulatory proteins, which caused the suppression of the PI3K/AκT pathway also via decreased integrin expression. These results hint at the potential of digitoxin and D6MA to shift the phenotype of cancerous cells toward an epithelial-like state, indicating the potential use of CGs or synthetic analogs as therapeutic agents for the treatment of lung cancer.

Funding

This work was supported through National Science Foundation (NSF) Grant Nos. 1434503, 1565788, and 1454230, the National Institutes of Health (ES022968), and NIOSH NTRC (921043S).

Data availability

A majority of the data that support the findings of this study are available from the corresponding authors upon reasonable request. The global genome data that support the findings will be available in NCBI GEO following an embargo from the date of publication.

Author contributions

R.E.D., A.W., C.D., and N.G. performed research and analyzed data; Y.R. and G.OD.-contributed with D6MA product and technical expertise, T.A.S. and C.Z.D. designed research; R.E.D., A.W., T.A.S. and C.Z.D. wrote the paper; all authors approved the paper.

Declaration of Competing Interest

The authors declare that they have no known competing financial interests or personal relationships that could have appeared to influence the work reported in this paper.

Acknowledgements

The findings and conclusions in this article are those of the authors and do not necessarily represent the view of the National Institute for Occupational Safety and Health (NIOSH), Centers for Disease Control and Prevention. Mention of product names does not constitute endorsement. The authors state that they have no conflicts of interest to declare.

Appendix A. Supplementary data

Supplementary data to this article can be found online at https://doi.org/10.1016/j.bbagen.2020.129683.

References

[1] M.H. Osman, E. Farrag, M. Selim, M.S. Osman, A. Hasanine, A. Selim, Cardiac glycosides use and the risk and mortality of cancer; systematic review and meta-analysis of observational studies, PLoS ONE 12 (6) (2017) e0178611.
[2] S. Frese, M. Frese-Schaper, A.C. Andres, D. Miescher, B. Zumkehr, R.A. Schmid, Cardiac glycosides initiate Apo2L/TRAIL-induced apoptosis in non-small cell lung cancer cells by up-regulation of death receptors 4 and 5, Cancer Res. 66 (11) (2006) 5867–5874.
[3] A.M. Katz, Effects of digitalis on cell biochemistry: sodium pump inhibition, J. Am. Coll. Cardiol. (5) (1985) 16A–21A.
[4] N. Arispe, J.C. Diaz, O. Simakova, H.B. Pollard, Heart failure drug digitoxin induces calcium uptake into cells by forming transmembrane calcium channels, Proc. Natl. Acad. Sci. U. S. A. 105 (7) (2008) 2610–2615.
[5] G. O'Doherty, M. Zhou, The de novo synthesis of oligosaccharides: application to the medicinal chemistry SAR-study of digitoxin, Curr. Top. Med. Chem. 8 (2) (2008) 114–125.
[6] H.A. Elbaz, T.A. Stueckle, H.Y. Wang, G.A. O'Doherty, D.T. Lowry, L.M. Sargent, et al., Digitoxin and a synthetic monosaccharide analog inhibit cell viability in lung cancer cells, Toxicol. Appl. Pharmacol. 258 (1) (2012) 51–60.
[7] H.A. Elbaz, T.A. Stueckle, W. Tse, Y. Rojanasakul, C.Z. Dinu, Digitoxin and its analogs as novel cancer therapeutics, Exp. Hematol. Oncol. 1 (1) (2012) 4.
[8] Y. Ren, E.J.C. de Blanco, J.R. Fuchs, D.D. Soejarto, J.E. Burdette, S.M. Swanson, et al., Potential anticancer agents characterized from selected tropical plants, J. Nat. Prod. 82 (3) (2019) 657–679.
[9] M. Lo'pez-La'zaro, N. Pastor, S.S. Azrak, M.J. Ayuso, C.A. Austin, F. Corte's, Digitoxin inhibits the growth of cancer cell lines at concentrations commonly found in cardiac patients, J. Nat. Prod. 68 (2005) 1642–1645.
[10] V. Pongrakhananon, T.A. Stueckle, H.L. Wang, G.A. O'Doherty, C.Z. Dinu, P. Chanvorachote, et al., Monosaccharide digitoxin derivative sensitize human non-small cell lung cancer cells to anoikis through Mcl-1 proteasomal degradation, Biochem. Pharmacol. 88 (1) (2014) 23–35.
[11] A.K. Iyer, M. Zhou, N. Azad, H. Elbaz, L. Wang, D.K. Rogalsky, et al., A direct comparison of the anticancer activities of digitoxin MeON-neoglycosides and O-glycosides: oligosaccharide chain length-dependent induction of caspase-9-mediated apoptosis, ACS Med. Chem. Lett. 1 (7) (2010) 326–330.
[12] R.A. Newman, P. Yang, A.D. Pawlus, K.I. Block, Cardiac glycosides as novel cancer therapeutic agents, Mol. Interv. 8 (1) (2008) 36–49.
[13] R. Eldawud, T.A. Stueckle, S. Manivanna, H. Elbaz, M. Chen, Y. Rojanasakul, et al., Real-time analysis of the effects of toxic, therapeutic and sub-therapeutic concentrations of digitoxin on lung cancer cells, Biosens. Bioelectron. 59 (2014) 192–199.
[14] T. Mijatovic, E. Van Quaquebeke, B. Delest, O. Debeir, F. Darro, R. Kiss, Cardiotonic steroids on the road to anti-cancer therapy, Biochim. Biophys. Acta 1776 (1) (2007) 32–57.
[15] H.Y. Wang, Y. Rojanasakul, G.A. O'Doherty, Synthesis and evaluation of the alpha-D−/alpha-L-rhamnosyl and amicetosyl digitoxigenin oligomers as anti-tumor agents, ACS Med. Chem. Lett. 2 (4) (2011) 264–269.
[16] H.-Y.L. Wang, W. Xin, M. Zhou, T.A. Stueckle, Y. Rojanasakul, G.A. O'Doherty, Stereochemical survey of digitoxin monosaccharides, ACS Med. Chem. Lett. 2 (1) (2010) 73–78.
[17] H.Y. Wang, Z. Qi, B. Wu, S.W. Kang, Y. Rojanasakul, G.A. O'Doherty, C5'-alkyl substitution effects on digitoxigenin alpha-l-glycoside cancer cytotoxicity, ACS Med. Chem. Lett. 2 (4) (2011) 259–263.
[18] S.O. Bajaj, J.R. Farnsworth, G.A. O'Doherty, Enantioselective synthesis of a- and b-Boc-protected 6-hydroxy pyranones: carbohydrate building blocks, Org. Synth. 91 (2014) 338–355.
[19] R.S. Babu, G.A. O'Doherty, A palladium-catalyzed glycosylation reaction: the de novo synthesis of natural and unnatural glycosides, J. Am. Chem. Soc. 125 (41) (2003) 12406–12407.
[20] M. Zhou, G. O'Doherty, The de novo synthesis of oligosaccharides: application to the medicinal chemistry SAR-study of digitoxin, Curr. Top. Med. Chem. 8 (2) (2008) 114–125.
[21] J.D. Baggot, L.E. Davis, Plasma protein binding of digitoxin and digoxin in several mammalian species, Res. Vet. Sci. 15 (1) (1973) 81–87.
[22] C. Lo, C.R. Keese, I. Giaever, Impedance analysis of MDCK cells measured by electric cell-substrate impedance sensing, Biophys. J. 69 (1995) 2800–2807.
[23] C. Rotsch, K. Jacobson, M. Radmacher, Dimensional and mechanical dynamics of active and stable edges in motile fibroblasts investigated by using atomic force microscopy, Proc. Natl. Acad. Sci. U. S. A. 96 (3) (1999) 921–926.
[24] A.B. Mathur, G.A. Truskey, W.M. Reichert, Atomic force and total internal reflection fluorescence microscopy for the study of force transmission in endothelial cells, Biophys. J. 78 (4) (2000) 1725–1735.
[25] M. Radmacher, M. Fritz, C.M. Kacher, J.P. Cleveland, P.K. Hansma, Measuring the viscoelastic properties of human platelets with the atomic force microscope, Biophys. J. 70 (1) (1996) 556–567.
[26] V.M. Laurent, S. Kasas, A. Yersin, T.E. Schaffer, S. Catsicas, G. Dietler, et al., Gradient of rigidity in the lamellipodia of migrating cells revealed by atomic force microscopy, Biophys. J. 89 (1) (2005) 667–675.
[27] T.G. Kuznetsova, M.N. Starodubtseva, N.I. Yegorenkov, S.A. Chizhik, R.I. Zhdanov, Atomic force microscopy probing of cell elasticity, Micron. 38 (8) (2007) 824–833.
[28] L. Wang, T.A. Stueckle, A. Mishra, R. Derk, T. Meighan, V. Castranova, et al., Neoplastic-like transformation effect of single-walled and multi-walled carbon nanotubes compared to asbestos on human lung small airway epithelial cells, Nanotoxicology. 8 (5) (2014) 485–507.
[29] X.J. Liang, C. Chen, Y. Zhao, P.C. Wang, Circumventing tumor resistance to chemotherapy by nanotechnology, Methods Mol. Biol. 596 (2010) 467–488.
[30] Y. Park, D. Kim, J. Dai, Z. Zhang, Human bronchial epithelial BEAS-2B cells, an appropriate in vitro model to study heavy metals induced carcinogenesis, Toxicol. Appl. Pharmacol. 287 (2015) 240–245.
[31] B. Xi, N. Yu, X. Wang, X. Xu, Y.A. Abassi, The application of cell-based label-free technology in drug discovery, Biotechnol. J. 3 (2008) 484–495.
[32] I. Giaever, C.R. Keese, A morphological biosensor for mammalian cells, Nature. 366 (1993) 591–592.
[33] J. Wegener, C.R. Keese, I. Giaever, Electric cell-substrate impedance sensing (ECIS) as a noninvasive means to monitor the kinetics of cell spreading to artificial surfaces, Exp. Cell Res. 259 (1) (2000) 158–166.
[34] H. Sabe, Cancer early dissemination: cancerous epithelial-mesenchymal transdifferentiation and transforming growth factor beta signalling, J. Biochem. 149 (6) (2011) 633–639.
[35] G.P. Gupta, J. Massague, Cancer metastasis: building a framework, Cell. 127 (4) (2006) 679–695.
[36] I. Giaever, C.R. Keese, Micromotion of mammalian cells measured electrically, Proc. Natl. Acad. Sci. 88 (1991) 7896–7900.
[37] J. Wegener, C.R. Keese, I. Giaever, Electric cell-substrate impedance sensing (ECIS) as a noninvasive means to monitor the kinetics of cell spreading to artificial surfaces, Exp. Cell Res. 259 (1) (2000) 158–166.
[38] M. Lopez-Lazaro, N. Pastor, S.S. Azrak, M.J. Ayuso, C.A. Austin, F. Cortes, Digitoxin inhibits the growth of cancer cell lines at concentrations commonly found in cardiac patients, J. Nat. Prod. 68 (2005) 1642–1645.
[39] R. Eldawud, T.A. Stueckle, S. Manivannan, H. Elbaz, M. Chen, Y. Rojanasakul, et al., Real-time analysis of the effects of toxic, therapeutic and sub-therapeutic concentrations of digitoxin on lung cancer cells, Biosens. Bioelectron. 59 (2014) 192–199.
[40] H.A. Elbaz, T.A. Stueckle, H.-Y.L. Wang, G.A. O'Doherty, D.T. Lowry, L.M. Sargent, et al., Digitoxin and a synthetic monosaccharide analog inhibit cell viability in lung cancer cells, Toxicol. Appl. Pharmacol. 258 (1) (2012) 51–60.
[41] R. Szulcek, H.J. Bogaard, G.P. van Nieuw Amerongen, Electric cell-substrate impedance sensing for the quantification of endothelial proliferation, barrier function, and motility, J. Visual. Exp. (2014) 85.
[42] D. Opp, B. Wafula, J. Lim, E. Huang, J.C. Lo, C.M. Lo, Use of electric cell-substrate impedance sensing to assess in vitro cytotoxicity, Biosens. Bioelectron. 24 (8) (2009) 2625–2629.
[43] C. Tiruppathi, A.B. Malik, P.J. Del Vecchio, C.R. Keese, I. Giaever, Electrical method for detection of endothelial cell shape change in real time: assessment of endothelial barrier function, Proc. Natl. Acad. Sci. U. S. A. 89 (1992) 7919–7923.
[44] A. Fuhrmann, A. Banisadr, P. Beri, T.D. Tlsty, A.J. Engler, Metastatic state of cancer cells may be indicated by adhesion strength, Biophys. J. 112 (4) (2017) 736–745.
[45] J.M. Caron, M. Bannon, L. Rosshirt, J. Luis, L. Monteagudo, G.M. Sternstein, Methyl sulfone induces loss of metastatic properties and reemergence of normal phenotypes in a metastatic cloudman S-91 (M3) murine melanoma cell line, PLoS ONE 5 (8) (2010) e11788.
[46] C. Xiao, J.H.T. Luong, Assessment of cytotoxicity by emerging impedance spectroscopy, Toxicol. Appl. Pharmacol. 206 (2) (2005) 102–112.

[47] F. Lautenschlager, S. Paschke, S. Schinkinger, A. Bruel, M. Beil, J. Guck, The regulatory role of cell mechanics for migration of differentiating myeloid cells, Proc. Natl. Acad. Sci. U. S. A. 106 (37) (2009) 15696–15701.
[48] C. De Pascalis, S. Etienne-Manneville, Single and collective cell migration: the mechanics of adhesions, Mol. Biol. Cell 28 (14) (2017) 1833–1846.
[49] Y. Shen, M. Leng, H. Yu, Q. Zhang, X. Luo, H. Gregersen, et al., Effect of amphiphilic PCL-PEG nano-micelles on HEpG2 cell migration, Macromol. Biosci. 15 (2015) 372–384.
[50] W. Gamal, S. Borooah, S. Smith, I. Underwood, V. Srsen, S. Chandran, et al., Real-time quantitative monitoring of hiPSC-based model of macular degeneration on electric cell-substrate impedance sensing microelectrodes, Biosens. Bioelectron. 71 (2015) 445–455.
[51] G. Forgacs, S.H. Yook, P.A. Janmey, H. Jeong, C.G. Burd, Role of the cytoskeleton in signaling networks, J. Cell Sci. 117 (2004) 2769–2775.
[52] G.M. Cooper, Signal Transduction and the Cytoskeleton, 2nd ed, Sinauer Associates, Sunderland (MA), 2000.
[53] M. Montes, E.A. Jaensson, A.F. Orozco, D.E. Lewis, D.B. Corry, A general method for bead-enhanced quantitation by flow cytometry, J. Immunol. Methods 317 (1–2) (2006) 45–55.
[54] P. Hyka, S. Lickova, P. Pribyl, K. Melzoch, K. Kovar, Flow cytometry for the development of biotechnological processes with microalgae, Biotechnol. Adv. 31 (1) (2013) 2–16.
[55] W.E. Crowe, N.K. Wills, A simple method for monitoring changes in cell height using fluorescent microbeads and an ussing-type chamber for the inverted microscope, Arch. Eur. J. Physiol. 419 (1991) 349–357.
[56] F. Re, A. Zanetti, M. Sironi, N. Polentarutti, L. Lanfrancone, E. Dejana, et al., Inhibition of anchorage-dependent cell spreading triggers apoptosis in cultured human endothelial cells, J. Cell Biol. 127 (1994) 537–546.
[57] M. Lekka, D. Gil, K. Pogoda, J. Dulinska-Litewka, R. Jach, J. Gostek, et al., Cancer cell detection in tissue sections using AFM, Arch. Biochem. Biophys. 518 (2) (2012) 151–156.
[58] T. Hawkins, M. Mirigian, M. Selcuk Yasar, J.L. Ross, Mechanics of microtubules, J. Biomech. 43 (1) (2010) 23–30.
[59] C. Dong, M.L. Kashon, D.T. Lowry, J.S. Dordick, S.H. Reynolds, Y. Rojanasakul, et al., Exposure to carbon nanotubes leads to changes in the cellular biomechanics, Adv. Healthc. Mat. 2 (2013) 1–7.
[60] Q. Luo, D. Kuang, B. Zhang, G. Song, Cell stiffness determined by atomic force microscopy and its correlation with cell motility, Biochim. Biophys. Acta Gen. Subj. 1860 (2016) 1953–1960.
[61] N. Guz, M. Dokukin, V. Kalaparthi, I. Sokolov, If cell mechanics can be described by elastic modulus: study of different models and probes used in indentation experiments, Biophys. J. 107 (3) (2014) 564–575.
[62] S.E. Cross, Y.S. Jin, J. Rao, J.K. Gimzewski, Nanomechanical analysis of cells from cancer patients, Nat. Nanotechnol. 2 (12) (2007) 780–783.
[63] C. Gialeli, A.D. Theocharis, N.K. Karamanos, Roles of matrix metalloproteinases in cancer progression and their pharmacological targeting, FEBS J. 278 (1) (2011) 16–27.
[64] G. Klein, E. Vellenga, M.W. Fraaije, W.A. Kamps, E.S. de Bont, The possible role of matrix metalloproteinase (MMP)-2 and MMP-9 in cancer, e.g. acute leukemia, Crit. Rev. Oncol. Hematol. 50 (2) (2004) 87–100.
[65] H.D. Foda, S. Zucker, Matrix metalloproteinases in cancer invasion, metastasis and angiogenesis, DDT. 6 (2001) 478–482.
[66] I. Stamenkovic, Matrix metalloproteinases in tumor invasion and metastasis, Semin. Cancer Biol. 10 (2000) 415–433.
[67] X. Xu, Y. Wang, Z. Chen, M.D. Sternlicht, M. Hidalgo, B. Steffensen, Matrix metalloproteinase-2 contributes to cancer cell migration on collagen, Cancer Res. 65 (2005) 130–136.
[68] A.J. Tsung, O. Kargiotis, C. Chetty, S.S. Lakka, M. Gujrati, D.G. Spomar, et al., Downregulation of matrix metalloproteinase-2 (MMP-2) utilizing adenovirus-mediated transfer of small interfering RNA (siRNA) in a novel spinal metastatic melanoma model, Int. J. Oncol. 32 (3) (2008) 557–564.
[69] C. Chetty, S.K. Vanamala, C.S. Gondi, D.H. Dinh, M. Gujrati, J.S. Rao, MMP-9 induces CD44 cleavage and CD44 mediated cell migration in glioblastoma xenograft cells, Cell. Signal. 24 (2) (2012) 549–559.
[70] M. Egeblad, Z. Werb, New functions for the matrix metalloproteinases in cancer progression, Nat. Rev. Cancer 2 (3) (2002) 161–174.
[71] A. Dufour, S. Zucker, N.S. Sampson, C. Kuscu, J. Cao, Role of matrix metalloproteinase-9 dimers in cell migration: design of inhibitory peptides, J. Biol. Chem. 285 (46) (2010) 35944–35956.
[72] J. Han, D.M. Rose, D.G. Woodside, L.E. Goldfinger, M.H. Ginsberg, Integrin alpha 4 beta 1-dependent T cell migration requires both phosphorylation and dephosphorylation of the alpha 4 cytoplasmic domain to regulate the reversible binding of paxillin, J. Biol. Chem. 278 (37) (2003) 34845–34853.
[73] P.D. Kassner, R. Alon, T.A. Springer, M.E. Hemler, Specialized functional properties of the integrin alpha4 cytoplasmic domain, Mol. Biol. Cell 6 (1995) 661–674.
[74] J.A. Varner, D.A. Cheresh, Integrins and cancer, Curr. Opin. Cell Biol. 8 (1996) 724–730.
[75] P. Huhtala, M.J. Humphries, J.B. McCarthy, P.M. Tremble, Z. Werb, C.H. Damsky, Cooperative signaling by α5β1and α4β1 Integrins regulates metalloproteinase gene expression in fibroblasts adhering to Fibronectin, J. Cell Biol. 129 (1995) 867–879.
[76] S. Silletti, T. Kessler, J. Goldberg, D.L. Boger, D.A. Cheresh, Disruption of matrix metalloproteinase 2 binding to integrin alpha vbeta 3 by an organic molecule inhibits angiogenesis and tumor growth in vivo, Proc. Natl. Acad. Sci. U. S. A. 98 (1) (2001) 119–124.
[77] E.I. Deryugina, M.A. Bourdon, K. Jungwirth, J.W. Smith, A.Y. Strongin, Functional activiation of integrin αVβ3 in tumor cells expressing membrane-type 1 matrix metalloproteinase, Int. J. Cancer 86 (2000) 15–23.
[78] P. Koistinen, J. Heino, Integrins in Cancer Cell Invasion, (2000–2013).
[79] Y. Zhang, C. Bao, Q. Mu, J. Chen, J. Wang, Y. Mi, et al., Reversal of cisplatin resistance by inhibiting PI3K/Akt signal pathway in human lung cancer cells, Neoplasma. 63 (3) (2016) 362–370.
[80] L. Ni, J. Lu, Interferon gamma in cancer immunotherapy, Cancer Med. 7 (9) (2018) 4509–4516.
[81] I. Prassas, G.S. Karagiannis, I. Batruch, A. Dimitromanolakis, A. Datti, E.P. Diamandis, Digitoxin-induced cytotoxicity in cancer cells is mediated through distinct kinase and interferon signaling networks, Mol. Cancer Ther. 10 (11) (2011) 2083–2093.
[82] L. Zhang, K. Nakaya, T. Yoshida, Y. Kuroiwa, Induction by bufalin of differentiation of human leukemia cells HL60, U937, and ML1 toward macrophage/monocyte-like cells and its potent synergistic effect on the differentiation of human leukemia cells in combination with other inducers, Cancer Res. 52 (17) (1992) 4634–4641.
[83] K. Czubak, M.A. Lewandowska, K. Klonowska, K. Roszkowski, J. Kowalewski, M. Figlerowicz, et al., High copy number variation of cancer-related microRNA genes and frequent amplification of DICER1 and DROSHA in lung cancer, Oncotarget. 6 (27) (2015) 23399–23416.
[84] K.S. Lee, Y.S. Lee, J.M. Lee, K. Ito, S. Cinghu, J.H. Kim, et al., Runx3 is required for the differentiation of lung epithelial cells and suppression of lung cancer, Oncogene. 29 (23) (2010) 3349–3361.
[85] W.L. Chen, Y. Ren, J. Ren, C. Erxleben, M.E. Johnson, S. Gentile, et al., (+)-Strebloside-induced cytotoxicity in ovarian Cancer cells is mediated through cardiac glycoside Signaling networks, J. Nat. Prod. 80 (3) (2017) 659–669.
[86] S. Honisch, S. Alkahtani, M. Kounenidakis, G. Liu, S. Alarifi, H. Al-Yahya, et al., A steroidal Na+/K+ ATPase inhibitor triggers pro-apoptotic signaling and induces apoptosis in prostate and lung tumor cells, Anti Cancer Agents Med. Chem. 14 (8) (2014) 1161–1168.
[87] T. Huang, L. Sun, X. Yuan, H. Qiu, Thrombospondin-1 is a multifaceted player in tumor progression, Oncotarget. 8 (48) (2017) 84546–84558.
[88] P.R. Halliday, C.M. Blakely, T.G. Bivona, Emerging targeted therapies for the treatment of non-small cell lung Cancer, Curr. Oncol. Rep. 21 (3) (2019) 21.
[89] M. Muramatsu, S. Akakura, L. Gao, J. Peresie, B. Balderman, I.H. Gelman, SSeCKS/Akap12 suppresses metastatic melanoma lung colonization by attenuating Src-mediated pre-metastatic niche crosstalk, Oncotarget. 9 (71) (2018) 33515–33527.
[90] Q. Lu, Delta-catenin dysregulation in cancer: interactions with E-cadherin and beyond, J. Pathol. 222 (2) (2010) 119–123.
[91] Q. Zhou, T. Chen, J.C. Ibe, J.U. Raj, G. Zhou, Knockdown of von Hippel-Lindau protein decreases lung cancer cell proliferation and colonization, FEBS Lett. 586 (10) (2012) 1510–1515.
[92] J. Redondo-Munoz, E. Escobar-Diaz, R. Samaniego, M.J. Terol, J.A. Garcia-Marco, A. Garcia-Pardo, MMP-9 in B-cell chronic lymphocytic leukemia is up-regulated by alpha4beta1 integrin or CXCR4 engagement via distinct signaling pathways, localizes to podosomes, and is involved in cell invasion and migration, Blood. 108 (9) (2006) 3143–3151.
[93] C.T. Chiu, J.H. Chen, F.P. Chou, H.H. Lin, Hibiscus sabdariffa leaf extract inhibits human prostate cancer cell invasion via down-regulation of Akt/NF-kB/MMP-9 pathway, Nutrients. 7 (7) (2015) 5065–5087.
[94] C.-Y. Cheng, H.-L. Hsieh, L.-D. Hsiao, C.-M. Yang, PI3-K/Akt/JNK/NF-κB is essential for MMP-9 expression and outgrowth in human limbal epithelial cells on intact amniotic membrane, Stem Cell Res. 9 (1) (2012) 9–23.
[95] M.L. Lin, Y.C. Lu, J.G. Chung, S.G. Wang, H.T. Lin, S.E. Kang, et al., Down-regulation of MMP-2 through the p38 MAPK-NF-kappaB-dependent pathway by aloe-emodin leads to inhibition of nasopharyngeal carcinoma cell invasion, Mol. Carcinog. 49 (9) (2010) 783–797.
[96] Z. Xie, T. Cai, Na+-K+–ATPase-mediated signal transduction: from protein interaction to cellular function, Mol. Interv. 3 (3) (2003) 157–168.
[97] J.E. Sero, H.Z. Sailem, R.C. Ardy, H. Almuttaqi, T. Zhang, C. Bakal, Cell shape and the microenvironment regulate nuclear translocation of NF-κB in breast epithelial and tumor cells, Mol. Syst. Biol. 11 (3) (2015) 790.
[98] M. Higuchi, K. Onishi, C. Kikuchi, Y. Gotoh, Scaffolding function of PAK in the PDK1-Akt pathway, Nat. Cell Biol. 10 (11) (2008) 1356–1364.
[99] N.M. Baker, H. Yee Chow, J. Chernoff, C.J. Der, Molecular pathways: targeting RAC-p21-activated serine-threonine kinase signaling in RAS-driven cancers, Clin. Cancer Res. 20 (18) (2014) 4740–4746.
[100] K. Thillai, H. Lam, D. Sarker, C.M. Wells, Deciphering the link between PI3K and PAK: an opportunity to target key pathways in pancreatic cancer? Oncotarget. 8 (8) (2017) 14173–14191.
[101] H.Y. Chow, B. Dong, C.A. Valencia, C.T. Zeng, J.N. Koch, T.Y. Prudnikova, et al., Group I Paks are essential for epithelial- mesenchymal transition in an Apc-driven model of colorectal cancer, Nat. Commun. 9 (1) (2018) 3473.
[102] Y.J. Wu, C.A. Neoh, C.Y. Tsao, J.H. Su, H.H. Li, Sinulariolide suppresses human hepatocellular carcinoma cell migration and invasion by inhibiting matrix Metalloproteinase-2/-9 through MAPKs and PI3K/Akt Signaling pathways, Int. J. Mol. Sci. 16 (7) (2015) 16469–16482.